Inherent losses induced absorptive acoustic rainbow trapping with a gradient metasurface

Cite as: J. Appl. Phys. **123**, 091702 (2018); https://doi.org/10.1063/1.4997631
Submitted: 25 July 2017 . Accepted: 07 September 2017 . Published Online: 19 December 2017

Tuo Liu, Shanjun Liang, Fei Chen, and Jie Zhu

Inherent losses induced absorptive acoustic rainbow trapping with a gradient metasurface

Tuo Liu, Shanjun Liang, Fei Chen, and Jie Zhu[a)]
Department of Mechanical Engineering, The Hong Kong Polytechnic University, Hung Hom, Kowloon, Hong Kong, China

(Received 25 July 2017; accepted 7 September 2017; published online 19 December 2017)

Acoustic rainbow trapping represents the phenomenon of strong acoustic dispersion similar to the optical "trapped rainbow," which allows spatial-spectral modulation and broadband trapping of sound. It can be realized with metamaterials that provide the required strong dispersion absent in natural materials. However, as the group velocity cannot be reduced to exactly zero before the forward mode being coupled to the backward mode, such trapping is temporary and the local sound oscillation ultimately radiates backward. Here, we propose a gradient metasurface, a rigid surface structured with gradient perforation along the wave propagation direction, in which the inherent thermal and viscous losses inside the holes are considered. We show that the gradually diminished group velocity of the structure-induced surface acoustic waves (SSAWs) supported by the metasurface becomes anomalous at the trapping position, induced by the existence of the inherent losses, which implies that the system's absorption reaches its maximum. Together with the progressively increased attenuation of the SSAWs along the gradient direction, reflectionless spatial-spectral modulation and sound enhancement are achieved in simulation. Such phenomenon, which we call as absorptive trapped rainbow, results from the balanced interplay among the local resonance inside individual holes, the mutual coupling of adjacent unit cells, and the inherent losses due to thermal conductivity and viscosity. This study deepens the understanding of the SSAWs propagation at a lossy metasurface and may contribute to the practical design of acoustic devices for high performance sensing and filtering. *Published by AIP Publishing*. https://doi.org/10.1063/1.4997631

I. INTRODUCTION

The concept of "rainbow trapping" or "trapped rainbow"[1,2] originated from the studies in quantum optics and nonlinear optics[3] on how to slow down and trap light. It was introduced to overcome the conflict subject to the causality between high optical delay and broad bandwidth. Different frequency components of broadband optical waves are decelerated until ultimately stopped at particular positions, leading to spatial-spectrally modulated and highly compressed optical field. Acoustic rainbow trapping (ART)[4–9] also received considerable interests as it innovates applications ranging from enhanced acoustic sensing and filtering[6] to broadband sound absorption.[8] Yet, distinct from electromagnetic waves, the lack of strong dispersion for sound in natural materials makes it more difficult to realize the trapped rainbow in the acoustic system.

Acoustic metamaterials and phononic crystals,[10–18] a class of promising artificially structured materials that possess exotic properties absent in nature, open doors to the on-demand dispersion engineering of acoustic waves. ART has since been theoretically and experimentally demonstrated with different metamaterial and phononic crystal designs.[4,5] Further efforts have been dedicated to make better utilization of space through space-coiling[7] and micro-Mie resonance-based units.[9] However, the group velocity of acoustic wave in these lossless metamaterial and phononic crystal models cannot be reduced to exactly zero due to the intermodal coupling between the forward and backward modes.[19] As a result, although the incident waves are slowed down and compressed to some degree, those localized sound fields will eventually radiate back rather than being permanently trapped. On the other hand, more and more researchers came to realize the importance of inherent losses on the performance of acoustic metamaterials[20–23] and spent great efforts in making full use of them to achieve a series of promising functions, e.g., deep subwavelength sound absorber,[24–27] metadiffuser,[28] and tunable asymmetric sound transmission.[29] Yet, the effect of inherent losses on ART structures has not been theoretically investigated in previous studies, which hampers their development for practical applications.

Here, we would like to take the intrinsic viscosity and thermal conductivity into consideration, to study a gradient metasurface for ART. In this case, incident acoustic waves parallel and close to the gradient metasurface can be effectively converted into the structure-induced surface acoustic mode with not only gradually compressed waveform but also progressively varied attenuation. At the trapping position, the inherent thermal and viscous losses dominate, playing an important role to balance the interplay between the local oscillation inside individual holes and the mutual coupling among neighboring units. The resultant dissipation helps to mitigate the backscattering so that a so-called absorptive trapped rainbow phenomenon can be observed. The proposed

[a)]Author to whom correspondence should be addressed: jie.zhu@polyu.edu.hk

gradient metasurface is a significant step towards the practical introduction of ART in high performance acoustic sensing and filtering. It may also help to design absorptive coatings to delay the hypersonic boundary layer transition.[30]

II. STRUCTURE-INDUCED SURFACE ACOUSTIC WAVES AT THE METASURFACE WITH INHERENT LOSSES

To achieve ART with a perforated metasurface, the key is to convert incident waves into the structure-induced surface acoustic waves (SSAWs) and manipulate its propagation. SSAWs, also referred to as spoof or designer surface acoustic waves and regarded as a counterpart of the structure-induced electromagnetic waves,[31] have been thoroughly investigated[32–42] and utilized in applications such as acoustic collimation,[33,34] focusing,[37] and imaging.[38] However, the effect of practical intrinsic losses due to thermal conductivity and viscosity on the SSAW propagation, a non-trivial factor for resonance structures,[20,21,23] has not been discussed until a very recent study given by Schwan *et al.*[42] They developed the theoretical model based on plane wave expansion and experimentally verified it, in which they showed that the slow acoustic surface mode is accompanied with strong attenuation, resulting in the diminished sound field away from the source. In this section, we follow the similar approach, but with a different way in obtaining the dispersion relation, that is, through analyzing the divergences of the reflection coefficient.[43] Here we focus on square holes whose depth h is several times larger than the lattice constant d, which is necessary for obtaining the enhanced sound field required by the ART effect.[4,6] As we demonstrate in the following, under such circumstance, the dispersion curve cannot reach the edge of the first Brillouin zone; namely, the maximum real part of the wave vector of the SSAWs $\mathrm{Re}(k_x)$ is lower than π/d. The group velocity consequently experiences an infinite point (a turning point in the dispersion curve), suggesting that the system's absorption reaches its maximum.[44,45]

Consider a rigid surface perforated with subwavelength square holes that are infinitely extended in x and y dimensions as shown in Fig. 1. The background medium (air) has density ρ_0 and sound speed c_0. The side length and depth of the holes are a and h, respectively, with the period of the unit cell being d. Assuming small-amplitude disturbance with time dependence $e^{j\omega t}$, the acoustic field of an arbitrary incident plane wave penetrating to the surface can be expressed as

$$p_i = e^{-jk_x x} e^{-jk_y y} e^{jk_z z}, \tag{1}$$

$$v_{z,i} = -\frac{1}{j\omega\rho_0}\frac{\partial p_i}{\partial z} = -\frac{k_z}{\rho_0\omega} e^{-jk_x x} e^{-jk_y y} e^{jk_z z}, \tag{2}$$

where p_i is the incident pressure, $v_{z,i}$ is the z-component of the particle velocity, and $j = \sqrt{-1}$. We define $q = \sqrt{k_x^2 + k_y^2}$ as the momentum parallel to the surface and $k_z = \sqrt{k_0^2 - q^2}$ as the perpendicular momentum, in which $k_0 = \omega/c_0$ is the wavenumber with ω being the angular frequency. The

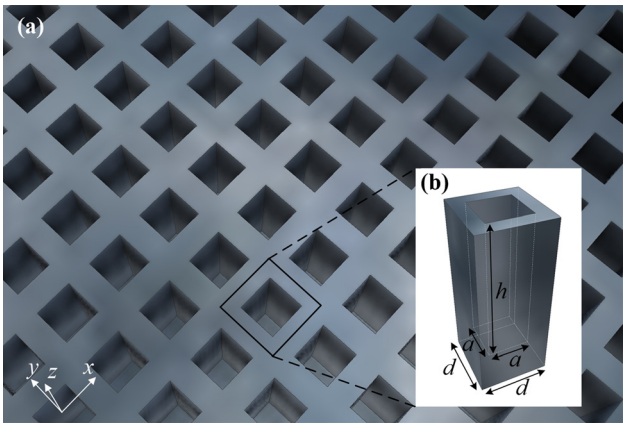

FIG. 1. Schematic illustration of (a) the metasurface and (b) a single unit cell. The metasurface is a rigid surface perforated with uniform subwavelength square holes. It is immersed in the air of density ρ_0 and sound speed c_0. The depth and side length of the holes are a and h, and the period of the unit cell is d, respectively. Inside the holes, since the thermal conductivity κ and viscosity μ are considered, the effective physical properties of density ρ_h, compressibility C_h, and wavenumber k_h are complex and frequency-dependent.

reflected pressure field $p_r^{(m,n)}$ and z-component particle velocity $v_{z,r}^{(m,n)}$ of the (m,n)-th order diffracted wave take the form

$$p_r^{(m,n)} = R_{mn} e^{-jk_x^{(m)} x} e^{-jk_y^{(n)} y} e^{-jk_z^{(m,n)} z}, \tag{3}$$

$$v_{z,r}^{(m,n)} = \frac{k_z^{(m,n)}}{\rho_0\omega} R_{mn} e^{-jk_x^{(m)} x} e^{-jk_y^{(n)} y} e^{-jk_z^{(m,n)} z}. \tag{4}$$

Here, $k_x^{(m)} = k_x + \frac{2\pi m}{d}$, $k_y^{(n)} = k_y + \frac{2\pi n}{d}$, and $k_z^{(m,n)} = \sqrt{k_0^2 - (k_x^{(m)})^2 - (k_y^{(n)})^2}$, $m, n = -\infty \ldots, -1, 0, 1, \ldots, +\infty$. R_{mn} is the reflection coefficient of the (m,n)-diffraction order, in which $(0,0)$ corresponds to the specular reflection.

Now we consider the losses that arise from thermal conductivity κ and viscosity μ inside the holes. As the side length of the square hole is much smaller than the wavelength ($a \ll \lambda$), inside these narrow regions, fundamental wave mode dominates at long wavelength limits, and the effective density ρ_h, compressibility C_h, and wavenumber k_h are complex and frequency-dependent in the presence of losses. Thus, the sound pressure and z-component particle velocity within the holes can be written as

$$p_h = C_1 e^{-jk_h z} + C_2 e^{jk_h z}, \tag{5}$$

$$v_{z,h} = \frac{k_h}{\rho_h\omega}(C_1 e^{-jk_h z} - C_2 e^{jk_h z}). \tag{6}$$

The complex coefficients in a tube of uniform cross-section are given by[46–48]

$$\rho_h(\omega) = \rho_0/\Psi_\nu, \quad C_h(\omega) = \frac{\gamma - (\gamma-1)\Psi_t}{\rho_0 c_0^2}, \tag{7}$$

$$k_h^2 = \omega^2 \rho_h(\omega) C_h(\omega) = k_0^2 \frac{\gamma - (\gamma-1)\Psi_t}{\Psi_\nu}, \tag{8}$$

in which for rectangular cross-section with side lengths a and b ($a = b$ in our model)

$$\Psi_{\mathrm{i}} = k_{\mathrm{i}}^2 \sum_{M=0}^{\infty} \left[\left(\frac{1}{\alpha_M M'} \right)^2 \left(1 - \frac{\tan(\alpha_M b/2)}{\alpha_M b/2} \right) + \left(\frac{1}{\beta_M M'} \right)^2 \left(1 - \frac{\tan(\beta_M a/2)}{\beta_M a/2} \right) \right] \tag{9}$$

with

$$\alpha_M = \sqrt{k_{\mathrm{i}}^2 - (2M'/a)^2}, \quad \beta_M = \sqrt{k_{\mathrm{i}}^2 - (2M'/b)^2},$$
$$M' = \left(M + \frac{1}{2} \right) \pi, \quad (M = 0, 1, 2, \ldots),$$

and

$$k_{\mathrm{i}}^2 = \begin{cases} k_v^2 = -j\omega \dfrac{\rho_0}{\mu}, & \text{viscous wave number} \\ k_t^2 = -j\omega \dfrac{\rho_0 C_p}{\kappa}, & \text{thermal wave number.} \end{cases} \tag{10}$$

Subscript i is either v or t that denotes the effect of viscous or thermal boundary layer. Here, $\gamma = C_P/C_V$ is the ratio of the specific heat at constant pressure C_P and the specific heat at constant volume C_V.

The bottom of the hole is rigid ($v_{z,h}|_{z=-h} = 0$) and thus we have $C_2 = C_1 e^{2jk_h h} \equiv C e^{2jk_h h}$. At the interface, the continuity condition of sound pressure for $a \ll \lambda$ requires that the mean pressure over the opening area at $z = 0^+$ equals the pressure inside the holes at $z = 0^-$, which is applied to obtain

$$\frac{1}{a^2} \int_{x,y=-a/2}^{x,y=a/2} \left(e^{-jk_x x} e^{-jk_y y} + \sum_{m,n=-\infty}^{+\infty} R_{mn} e^{-jk_x^{(m)} x} e^{-jk_y^{(n)} y} \right) \mathrm{d}x\mathrm{d}y = C(1 + e^{2jk_h h}). \tag{11}$$

After derivation, we have

$$\sum_{m,n=-\infty}^{+\infty} (\delta_{mn,00} + R_{mn}) S_{mn} = C(1 + e^{2jk_h h}), \tag{12}$$

where $S_{mn} = a^{-2} \int_{-\frac{a}{2}}^{\frac{a}{2}} e^{-jk_x^{(m)} x} \mathrm{d}x \int_{-\frac{a}{2}}^{\frac{a}{2}} \mathrm{d}y\, e^{-jk_y^{(n)} y} = \mathrm{sinc}(k_x^{(m)} a/2)\, \mathrm{sinc}(k_y^{(n)} a/2)$ is the overlap integral between the (m, n)-th order diffracted mode and the fundamental mode inside the holes; $\delta_{mn,00}$ is the Kronecker delta function defined as $\delta_{mn,00} = 1$ for $(m, n) = (0, 0)$ otherwise $\delta_{mn,00} = 0$. The particle velocity $v_z|_{z=0}$ must be continuous at the opening area while equals to zero elsewhere

$$-\frac{k_z}{\rho_0 \omega} e^{-jk_x x} e^{-jk_y y} + \sum_{m,n=-\infty}^{+\infty} \frac{k_z^{(m,n)}}{\rho_0 \omega} R_{mn} e^{-jk_x^{(m)} x} e^{-jk_y^{(n)} y} = \begin{cases} \dfrac{k_h}{\rho_h \omega} C(1 - e^{2jk_h h}) & x, y \in \left(-\dfrac{a}{2}, -\dfrac{a}{2} \right) \\ 0 & x, y \notin \left(-\dfrac{a}{2}, -\dfrac{a}{2} \right). \end{cases} \tag{13}$$

We multiply the above equation by $e^{jk_x^{(r)} x} e^{jk_y^{(s)} y}$ (r and s are integers) and average over the unit cell area

$$\frac{1}{d^2} \sum_{m,n=-\infty}^{+\infty} \int_{x,y=-d/2}^{x,y=d/2} \frac{k_z^{(m,n)}}{\rho_0 \omega} (R_{mn} - \delta_{mn,00}) \times e^{-j(k_x^{(m)} - k_x^{(r)}) x} e^{-j(k_y^{(n)} - k_y^{(s)}) y} \mathrm{d}x\mathrm{d}y = \frac{1}{d^2} \int_{x,y=-a/2}^{x,y=a/2} \frac{k_h}{\rho_h \omega} C(1 - e^{2jk_h h}) e^{jk_x^{(r)} x} e^{jk_y^{(s)} y} \mathrm{d}x\mathrm{d}y. \tag{14}$$

Based on the orthogonality of the exponential function, Eq. (14) can be derived as

$$R_{rs} = \delta_{rs,00} + C(1 - e^{2jk_h h}) \frac{a^2}{d^2} \frac{\rho_0 k_h}{\rho_h k_z^{(r,s)}} S_{rs}^*, \tag{15}$$

where $S_{rs}^* = a^{-2} \int_{-\frac{a}{2}}^{\frac{a}{2}} e^{jk_x^{(r)} x} \mathrm{d}x \int_{-\frac{a}{2}}^{\frac{a}{2}} \mathrm{d}y\, e^{jk_y^{(s)} y} = \mathrm{sinc}(k_x^{(r)} a/2)\, \mathrm{sinc}(k_y^{(s)} a/2)$. Substituting Eq. (15) into Eq. (12) yields

$$2S_{00} + C(1 - e^{2jk_h h}) \frac{\rho_0 a^2}{\rho_h d^2} \sum_{r,s=-\infty}^{+\infty} \frac{k_h}{k_z^{(r,s)}} S_{rs}^* S_{rs} = C(1 + e^{2jk_h h}). \tag{16}$$

The coefficient C is then determined as

$$C = \frac{2S_{00}}{(1 + e^{2jk_h h}) - (1 - e^{2jk_h h}) \dfrac{\rho_0 a^2}{\rho_h d^2} \displaystyle\sum_{r,s=-\infty}^{+\infty} \frac{k_h}{k_z^{(r,s)}} S_{rs}^* S_{rs}}. \tag{17}$$

The reflection coefficients in Eq. (15) can thus be expressed as

$$R_{mn} = \delta_{mn,00} + \frac{2(1 - e^{2jk_h h}) \dfrac{a^2}{d^2} \dfrac{\rho_0 k_h}{\rho_h k_z^{(m,n)}} S_{mn}^* S_{00}}{(1 + e^{2jk_h h}) - \dfrac{\rho_0 a^2}{\rho_h d^2} (1 - e^{2jk_h h}) \displaystyle\sum_{r,s=-\infty}^{+\infty} \frac{k_h}{k_z^{(r,s)}} S_{rs}^* S_{rs}}. \tag{18}$$

Here, we note that $-j \tan(k_h h) = \frac{1 - e^{2jk_h h}}{1 + e^{2jk_h h}}$ and $S_{rs}^* = S_{rs} = \mathrm{sinc}(k_x^{(r)} a/2) \mathrm{sinc}(k_y^{(s)} a/2)$. Equation (18) is simplified into the form

$$R_{mn} = \delta_{mn,00} - \frac{2j \tan(k_h h) \dfrac{\rho_0 a^2}{\rho_h d^2} S_{00} S_{mn} \dfrac{k_h}{k_z^{(m,n)}}}{1 + j \tan(k_h h) \dfrac{\rho_0 a^2}{\rho_h d^2} \cdot \displaystyle\sum_{r,s=-\infty}^{+\infty} \frac{k_h}{k_z^{(r,s)}} S_{rs}^2}. \tag{19}$$

A structure-induced surface mode is propagative along the parallel directions within the xy-plane, which requires $\mathrm{Re}(q) > k_0 > 0$ with $\mathrm{Re}(k_x) \geq 0$ and $\mathrm{Re}(k_y) \geq 0$. Meanwhile, it should be evanescent along the perpendicular direction z so that $\mathrm{Re}(jk_z) > 0$. For the lossy case, the propagation is with intrinsic attenuation, corresponding to $\mathrm{Im}(q) < 0 (\mathrm{Im}(k_x) \leq 0$ and $\mathrm{Im}(k_y) \leq 0)$. Therefore, setting $jk_z^{(r,s)} = \sqrt{(k_x^{(r)})^2 + (k_y^{(s)})^2 - k_0^2}$, the dispersion relation of the SSAWs can be obtained by analyzing the divergences of the $(0, 0)$-th order reflection coefficient,[43] namely, the zeros of the denominator of Eq. (19)

$$1 - k_h \tan(k_h h)\frac{\rho_0 a^2}{\rho_h d^2} \cdot \sum_{r,s=-\infty}^{+\infty} \frac{S_{rs}^2}{\sqrt{(q^{(r,s)})^2 - k_0^2}} = 0, \qquad (20)$$

where $(q^{(r,s)})^2 = (k_x^{(r)})^2 + (k_y^{(s)})^2$. Clearly, for the lossy model in which ρ_h and k_h are complex, the wavenumber of the SSAWs q must be complex too. The propagation of the SSAWs is therefore with inherent attenuation owing to the thermal and viscous losses. Another important characteristic of the SSAW is that it becomes a leaky surface mode when inherent losses are considered, namely, the coefficient $jk_z = \sqrt{q^2 - k_0^2}$ in $e^{-jk_z z}$ is a complex number. Note that it radiates energy to the fundamental mode inside the holes rather than the bulk mode in the upper half space due to the fact that $\mathrm{Im}\left(\sqrt{q^2 - k_0^2}\right) < 0$. Hence, without any leakage to the upper half space, the attenuation of the SSAWs completely stems from the inherent thermal and viscous losses within the holes.

Now we conduct theoretical calculation based on Eq. (20) to obtain the dispersion relation of the SSAWs at a metasurface with uniform unit cells of $a = 3\,\mathrm{mm}$, $d = 5\,\mathrm{mm}$, and $h = 25\,\mathrm{mm}$.The physical properties of air at 20 °C and standard atmospheric pressure are $\rho_0 = 1.21\,\mathrm{kg/m^3}$, $c_0 = 343\,\mathrm{m/s}$, $\kappa = 0.0258\,\mathrm{W/m \cdot K}$, $\mu = 1.81 \times 10^{-5}\,\mathrm{kg/m \cdot s}$, $C_p = 1.005 \times 10^3\,\mathrm{J/kg \cdot K}$, and $\gamma = 1.4$. Meanwhile, we also perform three-dimensional full-wave simulations using COMSOL Multiphysics to examine the SSAW propagation at an actual metasurface. In our simulation model, we arrange 40 units along the wave propagation direction x to approximately mimic a large enough metasurface. Periodic boundary condition and perfectly matched layers are employed to imitate the infinitely repeated units in the transverse direction y and the semi-infinite half space $z > 0$, respectively. The thermal and viscous losses inside the holes are introduced through replacing the lossless acoustic properties with complex quantities given in Eqs. (7) and (8). To effectively generate the surface mode,[35,37–41] a line source is applied near the edge of the metasurface ($x = 0$ and $z = 0$) and infinitely extended in the y direction.

As shown in Fig. 2(a), at low frequency range, the real part curve of the lossy model (red solid line) overlaps with those of both the lossless case (blue solid line) and the background medium air (black solid line). It starts to deviate from the air line as the frequency rises, while remaining similar with the lossless case. But with the lossy metasurface, a progressively increased imaginary part is presented (red dashed line), indicating the attenuation of the propagating SSAWs, as validated by the simulated sound field in Figs. 2(b) and 2(c). It is worth noting that for the SSAWs travelling along the metasurface with inherent losses, the dispersion curve cannot approach the edge of the first Brillouin zone; namely, the maximum real part of the wave vector $\mathrm{Re}(k_x)$ in the first Brillouin zone is smaller than π/d. This is distinct from the dispersion curve of the lossless case: k_x is a purely real number in the first Brillouin zone; it increases with frequency and reaches the maximum value at the edge of the first Brillouin zone ($k_x \to \pi/d$). It is also different from the case of Ref. 42, in which a lossy metasurface with relatively shallow holes still allows $\mathrm{Re}(k_x)$ to approach the zone edge. In our case, a turning point of dispersion curve [the peak of the red solid line in Fig. 2(a)] that represents the existence of infinite group velocity $v_g = \mathrm{d}\omega/\mathrm{d}k \to \infty$ can be observed, followed by a rapid decline. As pointed out by Refs. 44 and 45, the group velocity in a lossy medium becomes abnormal (e.g., infinite or negative) for the frequency at which the attenuation is maximum. Since the attenuation of the SSAWs completely comes from the

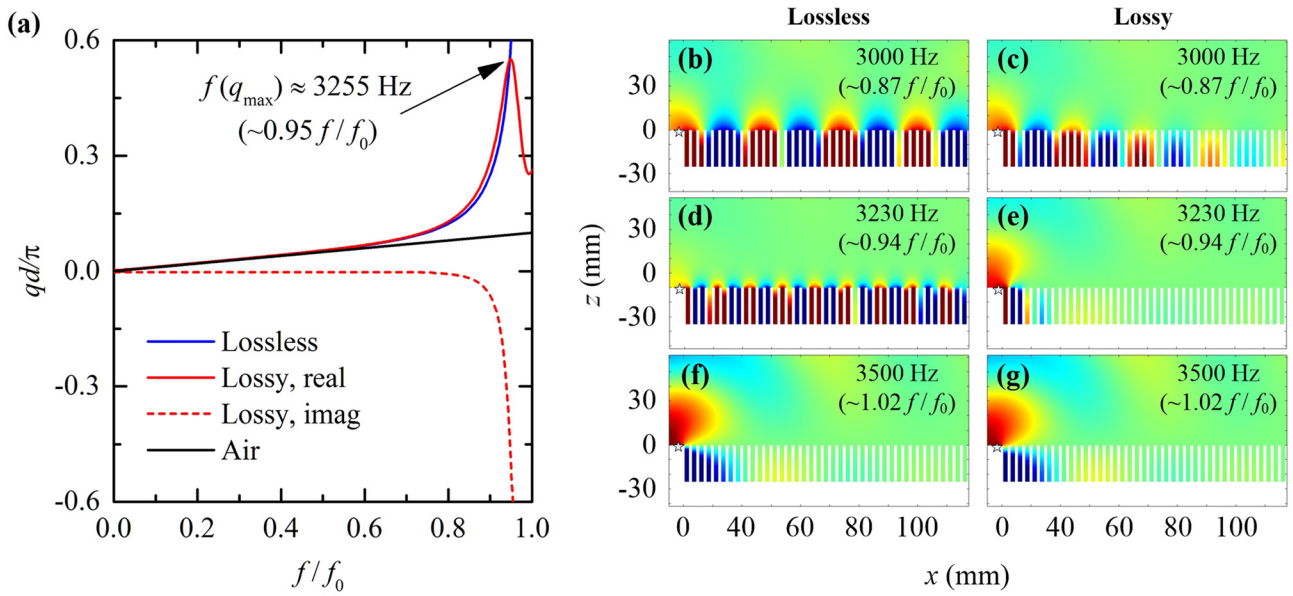

FIG. 2. Propagation characteristics of the structure-induced surface acoustic waves (SSAWs) at the metasurface with and without inherent losses. (a) Calculated dispersion relation of the SSAWs. The curves of the lossless case (blue solid line) and the air line (black solid line) are also presented. Here $f_0 = c_0/4h$ is the cavity resonance frequency. The unit cell is designed to have $a = 3\,\mathrm{mm}$, $d = 5\,\mathrm{mm}$, and $h = 25\,\mathrm{mm}$. (b)–(g) Simulated instantaneous acoustic pressure fields at three different frequencies for both lossless and lossy cases. The star in each subfigure represents a line source that is applied near the edge of the metasurface ($x = 0$ and $z = 0$) and infinitely extended in the y direction.

inherent thermal and viscous losses, such group velocity anomaly suggests that the absorption of the SSAWs reaches its maximum at the turning point. As shown in Fig. 2(e), the SSAWs are still propagative but with severe attenuation stemming from the absorption inside the unit cell holes, in stark contrast to the result of lossless model in Fig. 2(d). Beyond this turning point, the overwhelming imaginary part of the wavenumber becomes dominant, accounting for the stopband of the SSAWs. Accordingly, the surface mode can no longer be generated, as demonstrated in Figs. 2(f) and 2(g). For lossless case, the wavenumber is purely imaginary within the bandgap.

The frequency-dependent thermal and viscous losses can be directly tuned through adjusting the side length of the holes a, manifested by the complex wavenumber of sound waves travelling inside the holes k_h. They are related to the wavenumber of the SSAWs q through the dispersion relation given by Eq. (20). However, for the SSAW propagation, the side length a strongly affects not only the specific attenuation $2\pi\mathrm{Im}(q)/\mathrm{Re}(q)$ but also the real part of the wavenumber $\mathrm{Re}(q)$. This is to say that we are not able to independently tailor the attenuation without changing the real part of the dispersion curve. To demonstrate this, we calculate the dispersion curves of the SSAWs when a is set to 2.5 mm, 3 mm, and 3.5 mm, respectively ($d = 5$ mm and $h = 20$ mm). As shown in Fig. 3, a smaller a (black solid lines) would help to increase the attenuation of the SSAWs, but the highest value of $\mathrm{Re}(q)$ becomes smaller at the same time, suggesting that the SSAWs cannot be sufficiently slowed down and compressed; a higher value of $\mathrm{Re}(q)$ can be obtained with a larger hole size (blue solid lines), but with the downside of lower attenuation. Therefore, to find a balance between deceleration and attenuation of the SSAWs over a broad bandwidth, we select $a = 3$ mm for the gradient metasurface in Sec. III.

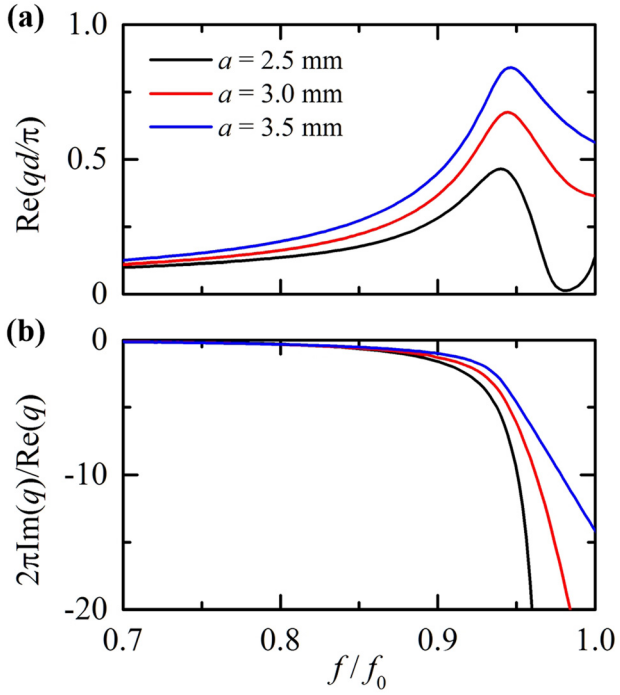

FIG. 3. Effects of different side lengths of the holes on the propagation characteristics of the SSAWs. (a) The real part of the SSAW wavenumber. (b) The specific attenuation of the SSAWs $2\pi\mathrm{Im}(q)/\mathrm{Re}(q)$. The unit cell is designed to have $d = 5$ mm and $h = 20$ mm. Black, red, and blue solid lines denote different side lengths of the holes 2.5 mm, 3.0 mm, and 3.5 mm, respectively.

III. ABSORPTIVE ACOUSTIC RAINBOW TRAPPING WITH GRADIENT METASURFACE

By arranging the hole depth distribution in a graded way along the wave propagation direction x as illustrated in Fig. 4(a), we construct the gradient metasurface that consists of 99 square holes with linear depth variation (0.25-mm step) ranging from 0.5 mm to 25 mm. Other properties are the same as those given above. It is worth mentioning that the variation of hole depth between neighboring units Δh should be much smaller than the lattice constant d to guarantee the gradually changed wavenumber of the SSAWs along the propagation direction. In other words, the propagation of the SSAWs from one unit to next unit is with very little mismatch of group velocity and attenuation. In our case, $\Delta h/d = 1/20$ is designed to meet this requirement. Such arrangement is equivalent to the so-called gradient-index design.[37,39,49] The dispersion curves corresponding to a series of uniform infinite metasurfaces constructed with different types of unit cells (different hole depths) are combined to obtain the spatial distributions of group velocity and attenuation. As shown in Fig. 4(b), each calculated group velocity of the SSAWs (solid lines) is equal to that of the background medium at $x = 0$ and gradually decreases to a non-zero minimum with the increase of horizontal position x. It then abruptly turns to infinity, suggesting that a cutoff corresponding to the trapping point exists and the absorption reaches maximum within this lossy system.[44,45] Such group velocity distribution is frequency dependent so that the reflectionless spatial-spectral separation becomes possible. Along with the strong attenuation of the SSAWs, the metasurface can act as an absorptive structure to mimic the "permanently" trapped rainbow. Here the quote mark is used to distinguish this trapping mechanism from the ideal ART model built with the effective medium that gradually reduces the group velocity to exactly zero.

We perform further numerical simulations to test the hypothesis. The settings are the same as those used in the model of metasurface with uniform holes except that the plane wave of unit amplitude travels from left to right [Fig. 5(a)] and interacts with the gradient metasurface.

As can be seen from the scattered and total instantaneous acoustic pressure fields at 5000 Hz in Figs. 5(b)–5(d), the incident wave near the surface is effectively converted into the SSAWs that are confined to the metasurface with the wavelength being highly compressed along the propagation direction, forming enhanced sound field. The maximum compression appears at the trapping position where the SSAWs cannot transmit further via diffractions so that the near-surface sound field beyond this trapping point becomes rather weak. Incident waves away from the surface cannot interact with the metasurface and thus continue to propagate without obvious wavefront change. For lossless case as

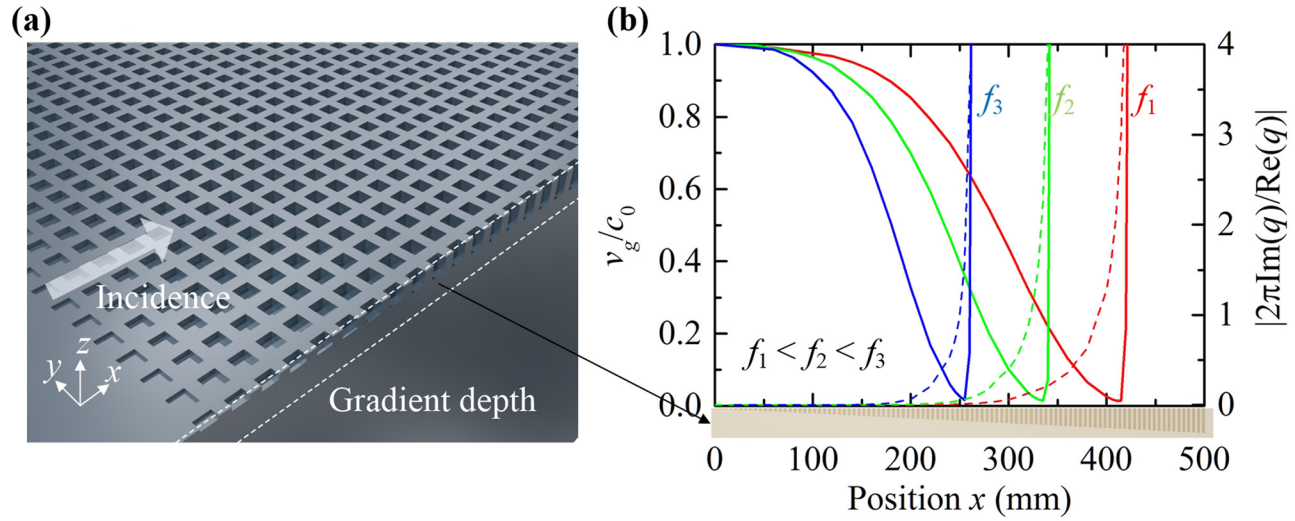

FIG. 4. Absorptive acoustic rainbow trapping (ART) with gradient metasurface. (a) Schematic illustration of the gradient metasurface. It consists of 99 graded square holes, whose depth linearly varied from 0.5 mm to 25 mm with a step 0.25 mm. (b) Group velocity and specific attenuation of the SSAWs along the gradient metasurface. The solid lines denote the group velocity and the dashed lines the absolute value of the specific attenuation (attenuation per wavelength). Red, green, and blue represent three different frequencies $f_1 = 3860$ Hz, $f_2 = 4730$ Hz, and $f_3 = 6110$ Hz. The group velocity anomaly (infinite) implies the maximum absorption of the lossy system.[44,45]

shown in Figs. 5(c) and 5(e), the deceleration of the SSAWs is restricted by the non-zero group velocity subject to intermodal coupling between forward and backward modes.[19] Hence the trapping is only temporarily achieved and the SSAWs are eventually reflected back to the half space. On the contrary, no obvious backscattering happens in the lossy model [Figs. 5(b) and 5(d)] so that an absorptive trapping phenomenon is observed. Such reflectionlessness behavior can be attributed to two facts: first, the conversion between incident plane waves and SSAWs experiences a gradual process as a result of the gradient distribution of group velocity that slowly drops from c_0 to the vicinity of zero with a very little mismatch along the x direction; second, the attenuation of the SSAWs also progressively increases during the propagation and becomes dominant at the trapping position so that the backward mode is nearly fully absorbed. It shows that the inherent losses due to viscosity and thermal conductivity help to rebuild the balanced interaction between the local oscillation inside individual holes and the mutual coupling among neighboring units.[4]

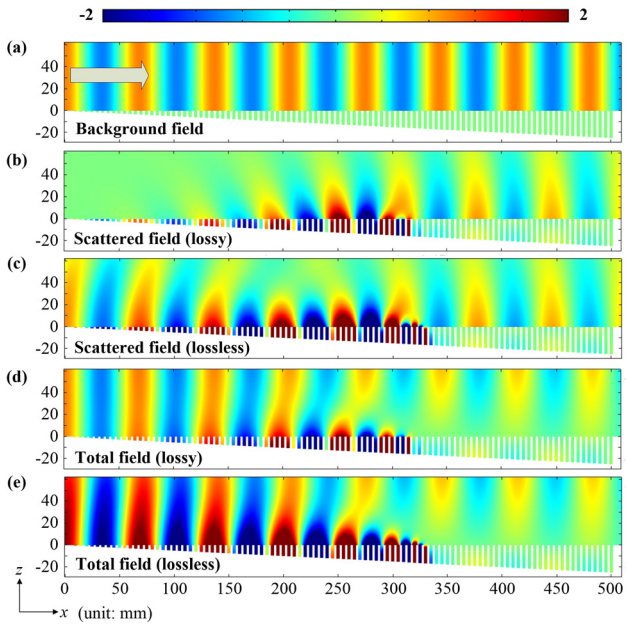

FIG. 5. Comparison of simulated instantaneous acoustic pressure fields of lossy and lossless models at 5000 Hz. (a) Background instantaneous acoustic field. The incident plane wave of unit amplitude travels from left-hand side to right-hand side. (b)–(e) Scattered and total instantaneous acoustic pressure fields of lossy and lossless models. The upper and lower limits of the acoustic pressure are set to two times the amplitude of the incident wave to guarantee that the wave pattern above the gradient metasurface is clear enough.

The simulated instantaneous and absolute total acoustic pressure fields at several different frequencies in the presence of losses are displayed in Fig. 6. The operating frequency increases linearly from Figs. 6(a) and 6(e) to Figs. 6(d) and 6(f). Incident waves of different frequencies are compressed and slowed down in different manners, depending on the spatial group velocity distributions shown in Fig. 4(b). The trapping happens at deeper holes for lower frequencies and at shallower holes for higher frequencies, which are determined by the group velocity anomaly points in space. The whole process generates hardly any backscattering. Otherwise, clear interference patterns would appear on the left-hand side of the absolute acoustic pressure fields [Figs. 6(e)–6(h)]. The overall phenomenon is in line with our theoretical expectation and confirms that the ART effect previously investigated in the lossless system[4] is still valid in the presence of inherent losses.

The spectral responses at the bottom of four holes located at different horizontal positions are also presented in Figs. 7(a) and 7(b). Compared to the lossless case (dashed lines in Fig. 7(a)), the oscillatory rise of pressure amplitude with respect to frequency is smoothed as a result of the vanished reflection. The enhancement of sound field, though weakened by the losses, still produces pressure amplitude more than ten times over the incident wave of unit amplitude.

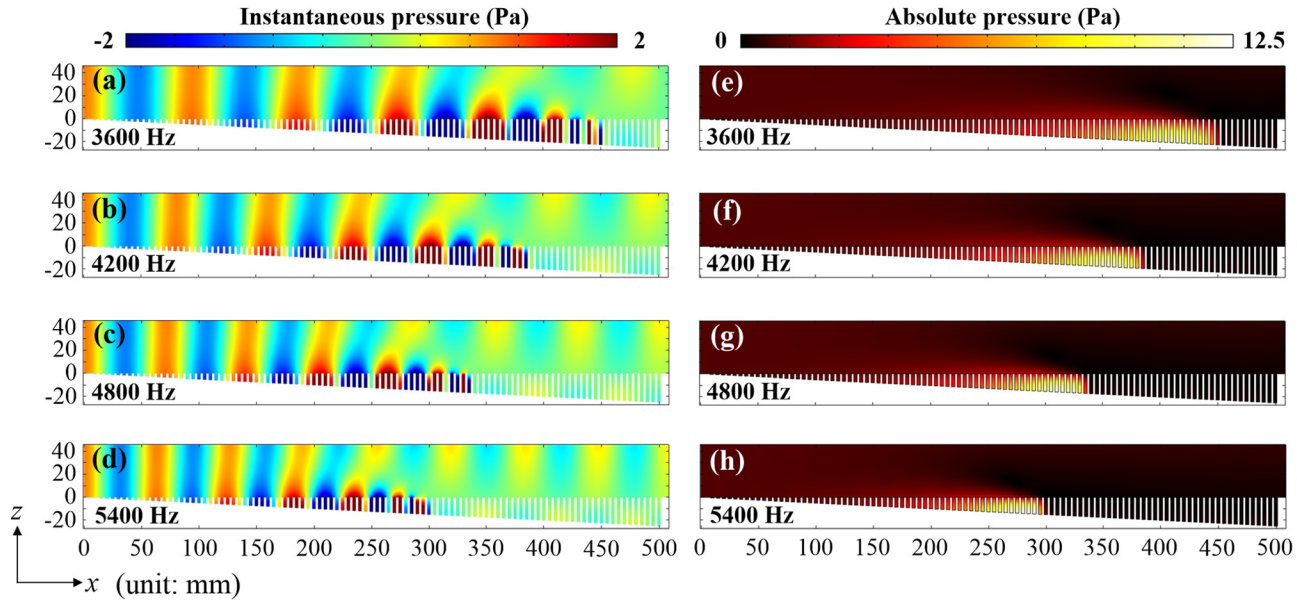

FIG. 6. Simulated instantaneous and absolute total acoustic pressure fields at several different frequencies in the presence of losses. (a)-(d) Instantaneous total acoustic pressure fields. The upper and lower limits of the acoustic pressure are set to two times the amplitude of the incident wave to guarantee that the wave pattern above the gradient metasurface is clear enough. (e)-(h) Absolute total acoustic pressure fields. The pressure amplitudes are normalized per the maximum among the results of the four frequencies.

In each curve of Fig. 7(a), the rapid decline of pressure amplitude after the peak forms a clear cutoff, indicating the so-called trapping point. From the lossless model (solid curves) to lossy model (dashed curves), these trapping points shift slightly towards low frequency range. This phenomenon originates from the changed propagation characteristics of the SSAWs caused by the inherent losses: the losses lead to complex effective wavenumber k_h and decreased speed of sound inside the holes, which lowers the resonance frequency;[20,21] since the SSAWs are a result of the interaction between the local resonance and the mutual coupling via diffractions, such change of resonance behavior consequently affects the propagation characteristics of the SSAWs. This overall shift is consistent with our theoretical prediction, as verified by the extracted trapping curves of Fig. 7(c), in which the lossy model offers a more accurate estimation as the losses are inherent and cannot be neglected in practice. It also provides a theoretical explanation to the deviation of the measured results from the lossless model in Ref. 4.

To further examine the backscattering from the trapping positions, we extracted the scattered pressure amplitude abs(p_{scat}) at several different heights within the upper half

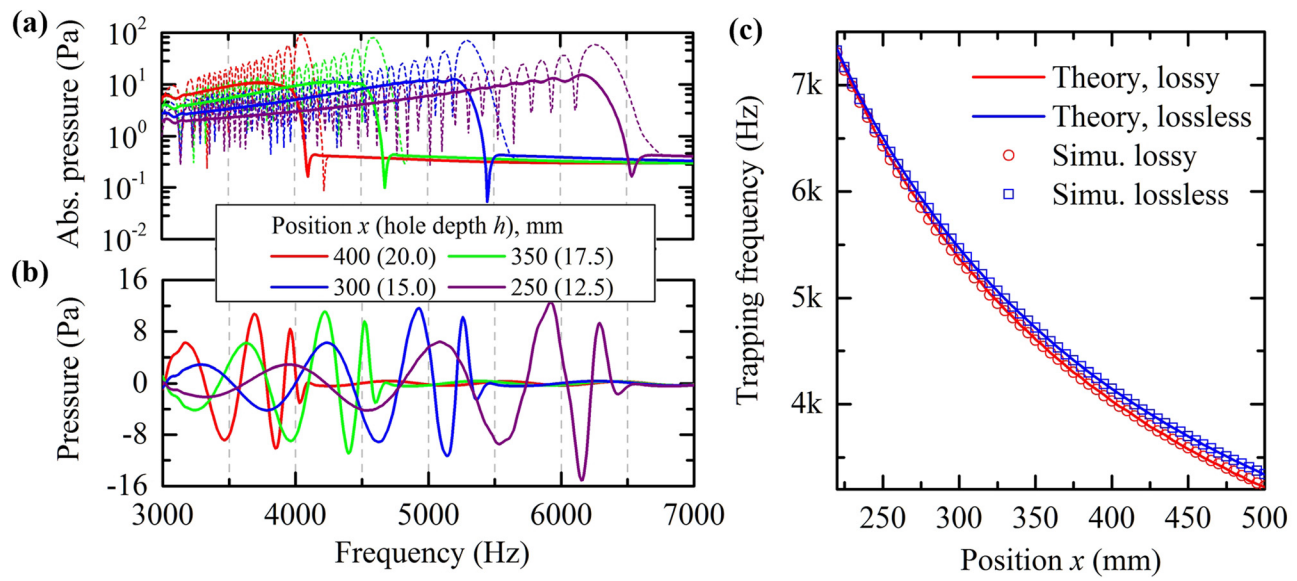

FIG. 7. Simulated frequency responses at the hole bottoms of four different horizontal positions and the extracted trapping curves. (a) Absolute acoustic pressure versus frequency. The results of lossless case are shown with dashed lines. (b) Instantaneous acoustic pressure versus frequency. In (a) and (b), different colors denote different horizontal positions. (c) Extracted trapping frequency versus position. The red and blue solid lines represent the theoretical calculations of lossy and lossless cases; circles and squares correspond to the simulation results of lossy and lossless cases.

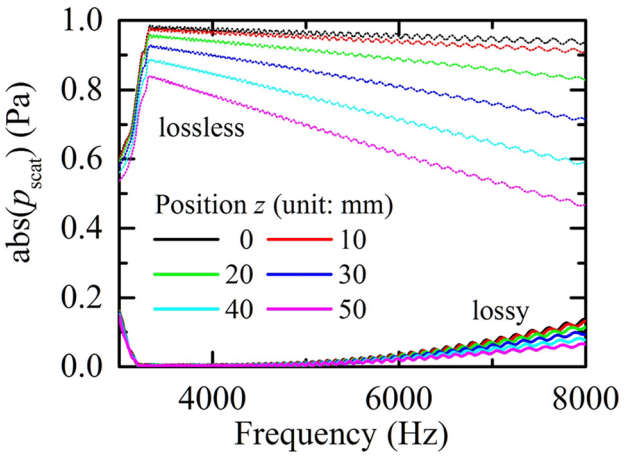

FIG. 8. Scattered acoustic pressure amplitudes versus frequency within the upper half space at $x = 0$. Different colors represent different heights away from the metasurface. The solid and dashed lines denote lossy and lossless cases, respectively.

space where $x = 0$. As shown in Fig. 8, the backscattering from the trapping positions is rather weak throughout the spectrum, which means that the SSAWs are truly trapped and absorbed inside the gradient metasurface. In contrast, the lossless perforated surface generates strong backscattering (dashed lines in Fig. 8) within the same frequency band, resulting from the intermodal coupling between the forward and backward modes. For higher frequencies, the attenuation of the SSAWs offered by the lossy metasurface becomes lower due to the decreased inherent losses inside the holes,[46–48] giving rise to gradually emerged (yet still much weaker than the lossless case) backscattering. Note that in lossless case the reduced backscattering along with the increased frequency comes from the weakened interaction between the incident wave and the structured surface since less units participate into the deceleration process. Such large distinction between the lossy and lossless cases testifies that the phenomenon presented in Figs. 5 and 6 is valid for a wide frequency range. It is evident that the inherent thermal and viscous losses play a key role to realize the absorptive ART, leading to the reflectionless spatial-spectral splitting and sound field enhancement.

From the physics point of view, the SSAWs are a result of the interplay between the local oscillation inside individual holes and the mutual coupling among adjacent units. The interplay forces the acoustic wave to travel in and out among the holes through diffractions. For a lossless case, the local oscillation experiences a process of periodic storage and release of energy subject to the operating frequency and strikes a balance with the mutual coupling at the resonance frequency.[4] While for a lossy case, the losses within the holes participate in the process and dissipate energy into heat. Such dissipation effect slowly becomes stronger along the direction where the hole depth increases, namely, along the wave propagation direction. At the trapping position, the local oscillation reaches resonance and the dissipation dominates, resulting in strong absorption of the surface mode. Therefore, the fundamental reason to absorb the SSAWs is the resonance behavior change of the units due to the inherent losses, together with the spatial modulation of the SSAWs offered by the gradient distribution of these units in space.

IV. CONCLUSIONS

In this study, we proposed a lossy gradient metasurface model to realize the absorptive acoustic rainbow trapping. The metasurface is constructed by arranging subwavelength square holes with a gradually increased depth along the wave propagation direction on a rigid surface. The inherent losses that originate from viscosity and thermal conductivity within the holes are now taken into consideration. Slowly diminished group velocity and progressively increased attenuation simultaneously happen along the metasurface for the structure-induced surface acoustic waves that are converted from the plane wave incidence. The group velocity becomes anomalous at the trapping position, leading to spatial-spectrally modulated and intensively enhanced sound field with vanished backscattering. The so-called absorptive trapped rainbow is thus realized. The proposed gradient metasurface can be used to design more practical devices for high performance sensing and detection. It may also provide the theoretical support to the study of absorptive coatings for stabilization of the hypersonic boundary layer.[30]

ACKNOWLEDGMENTS

The work was supported by the Early Career Scheme (ECS) of Hong Kong RGC (Grant No. 25208115) and the Departmental Internal Competitive Research Grant G-UA8T from the Hong Kong Polytechnic University.

[1]K. L. Tsakmakidis, A. D. Boardman, and O. Hess, "Trapped rainbow'storage of light in metamaterials," Nature **450**(7168), 397–401 (2007).
[2]Q. Gan, Y. J. Ding, and F. J. Bartoli, "Rainbow trapping and releasing at telecommunication wavelengths," Phys. Rev. Lett. **102**(5), 056801 (2009).
[3]T. F. Krauss, "Why do we need slow light?," Nat. Photonics **2**(8), 448–450 (2008).
[4]J. Zhu, Y. Chen, X. Zhu, F. J. Garcia-Vidal, X. Yin, W. Zhang, and X. Zhang, "Acoustic rainbow trapping," Sci. Rep. **3**, 1728 (2013).
[5]V. Romero-Garcia, R. Picó, A. Cebrecos, V. J. Sanchez-Morcillo, and K. Staliunas, "Enhancement of sound in chirped sonic crystals," Appl. Phys. Lett. **102**(9), 091906 (2013).
[6]Y. Chen, H. Liu, M. Reilly, H. Bae, and M. Yu, "Enhanced acoustic sensing through wave compression and pressure amplification in anisotropic metamaterials," Nat. Commun. **5**, 5247 (2014).
[7]X. Ni, Y. Wu, Z. G. Chen, L. Y. Zheng, Y. L. Xu, P. Nayar, X. P. Liu, M. H. Lu, and Y. F. Chen, "Acoustic rainbow trapping by coiling up space," Sci. Rep. **4**, 7038 (2014).
[8]X. Jiang, B. Liang, R. Q. Li, X. Y. Zou, L. L. Yin, and J. C. Cheng, "Ultra-broadband absorption by acoustic metamaterials," Appl. Phys. Lett. **105**(24), 243505 (2014).
[9]C. Zhou, B. Yuan, Y. Cheng, and X. Liu, "Precise rainbow trapping for low-frequency acoustic waves with micro mie resonance-based structures," Appl. Phys. Lett. **108**(6), 063501 (2016).
[10]Z. Liu, X. Zhang, Y. Mao, Y. Y. Zhu, Z. Yang, C. T. Chan, and P. Sheng, "Locally resonant sonic materials," Sci. **289**(5485), 1734–1736 (2000).
[11]J. Li and C. T. Chan, "Double-negative acoustic metamaterial," Phys. Rev. E **70**(5), 055602 (2004).
[12]N. Fang, D. Xi, J. Xu, M. Ambati, W. Srituravanich, C. Sun, and X. Zhang, "Ultrasonic metamaterials with negative modulus," Nat. Mater. **5**(6), 452–456 (2006).
[13]Z. Yang, J. Mei, M. Yang, N. H. Chan, and P. Sheng, "Membrane-type acoustic metamaterial with negative dynamic mass," Phys. Rev. Lett. **101**(20), 204301 (2008).

[14]J. Li, L. Fok, X. Yin, G. Bartal, and X. Zhang, "Experimental demonstration of an acoustic magnifying hyperlens," Nat. Mater. **8**(12), 931–934 (2009).
[15]B. Liang, X. S. Guo, J. Tu, D. Zhang, and J. C. Cheng, "An acoustic rectifier," Nat. Mater. **9**(12), 989–992 (2010).
[16]J. Zhu, J. Christensen, J. Jung, L. Martin-Moreno, X. Yin, L. Fok, X. Zhang, and F. J. Garcia-Vidal, "A holey-structured metamaterial for acoustic deep-subwavelength imaging," Nat. Phys. **7**(1), 52–55 (2011).
[17]X. Zhu, H. Ramezani, C. Shi, J. Zhu, and X. Zhang, "PT-symmetric acoustics," Phys. Rev. X **4**(3), 031042 (2014).
[18]Z. Yang, F. Gao, X. Shi, X. Lin, Z. Gao, Y. Chong, and B. Zhang, "Topological acoustics," Phys. Rev. Lett. **114**(11), 114301 (2015).
[19]S. He, Y. He, and Y. Jin, "Revealing the truth about 'trapped rainbow'storage of light in metamaterials," Sci. Rep. **2**, 583 (2012).
[20]G. P. Ward, R. K. Lovelock, A. R. J. Murray, A. P. Hibbins, J. R. Sambles, and J. D. Smith, "Boundary-layer effects on acoustic transmission through narrow slit cavities," Phys. Rev. Lett. **115**(4), 044302 (2015).
[21]M. Serra-Garcia and C. Daraio, "Visco-thermal effects in acoustic metamaterials: From total transmission to total reflection and high absorption," New J. Phys. **18**(3), 033003 (2016).
[22]X. Jiang, Y. Li, and L. Zhang, "Thermoviscous effects on sound transmission through a metasurface of hybrid resonances," J. Acoust. Soc. Am. **141**(4), EL363–EL368 (2017).
[23]V. C. Henríquez, V. M. García-Chocano, and J. Sánchez-Dehesa, "Viscothermal losses in double-negative acoustic metamaterials," Phys. Rev. Appl. **8**(1), 014029 (2017).
[24]A. Merkel, G. Theocharis, O. Richoux, V. Romero-García, and V. Pagneux, "Control of acoustic absorption in one-dimensional scattering by resonant scatterers," Appl. Phys. Lett. **107**(24), 244102 (2015).
[25]Y. Li and B. M. Assouar, "Acoustic metasurface-based perfect absorber with deep subwavelength thickness," Appl. Phys. Lett. **108**(6), 063502 (2016).
[26]N. Jiménez, W. Huang, V. Romero-García, V. Pagneux, and J. P. Groby, "Ultra-thin metamaterial for perfect and quasi-omnidirectional sound absorption," Appl. Phys. Lett. **109**(12), 121902 (2016).
[27]N. Jiménez, V. Romero-García, V. Pagneux, and J. P. Groby, "Quasiperfect absorption by subwavelength acoustic panels in transmission using accumulation of resonances due to slow sound," Phys. Rev. B **95**(1), 014205 (2017).
[28]N. Jiménez, T. J. Cox, V. Romero-García, and J. P. Groby, "Metadiffusers: Deep-subwavelength sound diffusers," Sci. Rep. **7**(1), 5389 (2017).
[29]Y. Li, C. Shen, Y. Xie, J. Li, W. Wang, S. A. Cummer, and Y. Jing, "Tunable asymmetric transmission via lossy acoustic metasurfaces," Phys. Rev. Lett. **119**(3), 035501 (2017).
[30]A. Fedorov, A. Shiplyuk, A. Maslov, E. Burov, and N. Malmuth, "Stabilization of a hypersonic boundary layer using an ultrasonically absorptive coating," J. Fluid Mech. **479**, 99–124 (2003).
[31]J. B. Pendry, L. Martin-Moreno, and F. J. Garcia-Vidal, "Mimicking surface plasmons with structured surfaces," Science **305**(5685), 847–848 (2004).
[32]L. Kelders, J. F. Allard, and W. Lauriks, "Ultrasonic surface waves above rectangular-groove gratings," J. Acoust. Soc. Am. **103**(5), 2730–2733 (1998).
[33]J. Christensen, A. I. Fernandez-Dominguez, F. de Leon-Perez, L. Martin-Moreno, and F. J. Garcia-Vidal, "Collimation of sound assisted by acoustic surface waves," Nat. Phys. **3**(12), 851–852 (2007).
[34]Y. Zhou, M. H. Lu, L. Feng, X. Ni, Y. F. Chen, Y. Y. Zhu, S. N. Zhu, and N. B. Ming, "Acoustic surface evanescent wave and its dominant contribution to extraordinary acoustic transmission and collimation of sound," Phys. Rev. Lett. **104**(16), 164301 (2010).
[35]Z. He, H. Jia, C. Qiu, Y. Ye, R. Hao, M. Ke, and Z. Liu, "Nonleaky surface acoustic waves on a textured rigid surface," Phys. Rev. B **83**(13), 132101 (2011).
[36]D. Torrent and J. Sánchez-Dehesa, "Acoustic analogue of graphene: Observation of Dirac cones in acoustic surface waves," Phys. Rev. Lett. **108**(17), 174301 (2012).
[37]Y. Ye, M. Ke, Y. Li, T. Wang, and Z. Liu, "Focusing of spoof surface-acoustic-waves by a gradient-index structure," J. Appl. Phys. **114**(15), 154504 (2013).
[38]H. Jia, M. Lu, Q. Wang, M. Bao, and X. Li, "Subwavelength imaging through spoof surface acoustic waves on a two-dimensional structured rigid surface," Appl. Phys. Lett. **103**(10), 103505 (2013).
[39]H. Jia, M. Lu, X. Ni, M. Bao, and X. Li, "Spatial separation of spoof surface acoustic waves on the graded groove grating," J. Appl. Phys. **116**(12), 124504 (2014).
[40]L. Quan, F. Qian, X. Liu, X. Gong, and P. A. Johnson, "Mimicking surface plasmons in acoustics at low frequency," Phys. Rev. B **92**(10), 104105 (2015).
[41]J. Lu, C. Qiu, M. Ke, and Z. Liu, "Directional excitation of the designer surface acoustic waves," Appl. Phys. Lett. **106**(20), 201901 (2015).
[42]L. Schwan, A. Geslain, V. Romero-García, and J. P. Groby, "Complex dispersion relation of surface acoustic waves at a lossy metasurface," Appl. Phys. Lett. **110**(5), 051902 (2017).
[43]F. J. Garcia-Vidal, L. Martin-Moreno, and J. B. Pendry, "Surfaces with holes in them: New plasmonic metamaterials," J. Opt. A: Pure Appl. Opt. **7**(2), S97 (2005).
[44]E. L. Bolda, R. Y. Chiao, and J. C. Garrison, "Two theorems for the group velocity in dispersive media," Phys. Rev. A **48**(5), 3890 (1993).
[45]P. W. Milonni, *Fast Light, Slow Light and Left-Handed Light* (CRC Press, 2004).
[46]C. Zwikker and C. W. Kosten, *Sound Absorbing Materials* (Elsevier, 1949).
[47]M. R. Stinson, "The propagation of plane sound waves in narrow and wide circular tubes, and generalization to uniform tubes of arbitrary cross-sectional shape," J. Acoust. Soc. Am. **89**(2), 550–558 (1991).
[48]V. F. Kozlov, A. V. Fedorov, and N. D. Malmuth, "Acoustic properties of rarefied gases inside pores of simple geometries," J. Acoust. Soc. Am. **117**(6), 3402–3411 (2005).
[49]S. C. S. Lin, T. J. Huang, J. H. Sun, and T. T. Wu, "Gradient-index phononic crystals," Phys. Rev. B **79**(9), 094302 (2009).